Electronic processes occurring during ultrafast demagnetization of cobalt triggered by x-ray photons tuned to the Co L_3 resonance

Konrad J. Kapcia,[1,2,*] Victor Tkachenko,[3,4,2,†] Flavio Capotondi,[5] Alexander Lichtenstein,[4,6] Serguei Molodtsov,[4,7,8] Leonard Mueller,[9] Andre Philippi-Kobs,[9] Przemysław Piekarz,[3] and Beata Ziaja[2,3,‡]

[1]*Institute of Spintronics and Quantum Information, Faculty of Physics, Adam Mickiewicz University in Poznań, Uniwersytetu Poznańskiego 2, 61614 Poznań, Poland*

[2]*Center for Free-Electron Laser Science CFEL, Deutsches Elektronen Synchrotron DESY, Notkestr. 85, 22607 Hamburg, Germany*

[3]*Institute of Nuclear Physics, Polish Academy of Sciences, Radzikowskiego 152, 31-342 Kraków, Poland*

[4]*European XFEL GmbH, Holzkoppel 4, 22869 Schenefeld, Germany*

[5]*Elettra-Sincrotrone Trieste S.C.p.A, 34149 Trieste, Basovizza, Italy*

[6]*Institute of Theoretical Physics, University of Hamburg, Jungiusstrasse 9, 20355 Hamburg, Germany*

[7]*Institute of Experimental Physics, TU Bergakademie Freiberg, Leipziger Strasse 23, 09599 Freiberg, Germany*

[8]*Center for Efficient High Temperature Processes and Materials Conversion (ZeHS), TU Bergakademie Freiberg, Winklerstrasse 5, 09599 Freiberg, Germany*

[9]*Deutsches Elektronen Synchrotron DESY, Notkestr. 85, 22607 Hamburg, Germany*

(Received 13 July 2022; revised 23 November 2022; accepted 14 February 2023; published 3 March 2023)

Magnetization dynamics triggered by ultrashort laser pulses has been attracting significant attention, with a strong focus on the dynamics excited by visible/near-infrared pulses. Only recently has a strong magnetic response in solid materials induced by intense x-ray pulses from free-electron lasers been observed. The exact mechanisms that trigger the x-ray-induced demagnetization are not yet fully understood. They are the subject of ongoing experimental and theoretical investigations. Here, we present a theoretical analysis of electronic processes occurring during demagnetization of a Co multilayer system irradiated by x-ray pulses tuned to the L_3 absorption edge of cobalt. We show that, like in the case of x-ray-induced demagnetization at the M edge of Co, electronic processes play a predominant role in the demagnetization until the pulse fluence does not exceed the structural damage threshold. The impact of electronic processes can explain reasonably well the available experimental data, without a need to introduce the mechanism of stimulated elastic forward scattering.

DOI: 10.1103/PhysRevB.107.094402

I. INTRODUCTION

Since its discovery [1], ultrafast demagnetization has been studied mostly with lasers working in the infrared regime [2–7]. X-ray-induced ultrafast demagnetization has become a topic of intense study after the commissioning of the new generation of light sources, x-ray and XUV free-electron lasers (FELs; see, e.g., [8–18]). The FELs produce ultrashort, intense, coherent, and wavelength-tunable x-ray pulses [19–22]. Such pulses provide an opportunity to study demagnetization by using the x-ray magnetic circular dichroism (XMCD) effect, with FEL photons of energy tuned to a dichroic absorption edge of a ferromagnetic element [3,23–27]. The principle of XMCD has been, in particular, explored using resonant magnetic small-angle x-ray scattering measurements [8,17,28], with which the magnetic response of irradiated systems can be probed on femtosecond timescales. The experiments which employed resonant magnetic scattering with photons tuned to the M absorption edge of cobalt, acting either as a pump or a probe, are described in Refs. [8,9,11,16,17]. The experiments which employed resonant magnetic x-ray scattering at the L absorption edge of cobalt are described in [10,13,15]. Similar studies were also performed for nickel samples [29,30].

The first theoretical explanation proposed for the observed loss of resonant magnetic scattering signal at the M edge of cobalt was proposed in [11]. The mechanism considered was the perturbation of the electronic state within the magnetic sample during the first few femtoseconds of exposure leading to the atomic levels shifts and to the resulting ultrafast quenching of the resonant magnetic scattering. However, the proposed mechanism was formulated in [11] as a hypothesis and was not proven explicitly there. In the following x-ray studies of the Co L edge [12,13,15], the decreasing magnetic scattering signal was explained via stimulated elastic forward scattering in a simplified two-level atom model. However, this approach did not provide a full treatment of radiation damage caused by incoming x-ray photons. In particular, the two-level model approach could not account for the effect of electrons released during x-ray irradiation on electronic occupations within the cobalt conduction band. Consequently, it did not accurately describe the magnetization dynamics triggered by photons tuned to the M edge of Co [17].

In Ref. [18], we proposed a modeling tool called XSPIN that enables a comprehensive nanoscopic description of electronic processes occurring in x-ray-irradiated ferromagnetic

*konrad.kapcia@amu.edu.pl
†victor.tkachenko@xfel.eu
‡ziaja@mail.desy.de

materials. With this tool, we studied the response of a Co/Pt multilayer system irradiated by an ultrafast XUV pulse tuned to the M edge of Co (photon energy $\sim$ 60 eV) under conditions corresponding to those of the experiment [17]. The XSPIN simulations showed that the magnetic scattering signal from cobalt decreased on femtosecond timescales due to electronic excitation, relaxation, and transport processes in both the cobalt and platinum layers. The signal decrease was stronger with increasing fluence of the incoming radiation, following the trend observed in the experimental data. Confirmation of the predominant role of electronic processes in x-ray-induced demagnetization in the regime below the structural damage threshold, which was achieved with our theoretical study, was a step towards quantitative understanding of x-ray-induced magnetic processes on femtosecond timescales.

In this work, we apply the XSPIN model to describe the results of the experiment on resonant x-ray scattering with photons tuned to the L_3 absorption edge of Co performed at the Linac Coherent Light Source (LCLS) free-electron laser facility and presented in Ref. [13]. Although the electron kinetics following Co irradiation with x-ray photons of $\sim$778 eV energy includes additional photoexcitation and relaxation channels such as inner-shell excitation and the resulting Auger processes, the electronic relaxation progresses in a way (through collisional processes) similar to that after Co irradiation with 60 eV photons (M-edge case). Our purpose is to show that the collisional electronic relaxation is a universal mechanism that can explain ultrafast demagnetization of Co by x-ray pulses of low fluence, independent of x-ray photon energy.

In what follows, we will recall the details of the measurement performed in [13] (Sec. II). Afterwards, we will discuss the application of the XSPIN model to model demagnetization induced by x-ray photons tuned to the Co L_3 edge (Sec. III). We will then present the model results compared to experimental data (Sec. IV). Finally, our conclusions will be listed (Sec. V). In the Appendixes, more details on our computational tools are presented.

II. RESONANT X-RAY SCATTERING EXPERIMENT AT THE LCLS FACILITY

In the experiment performed by Wu *et al.* at the LCLS facility [13], the Co/Pd magnetic multilayer system was used. The details are taken from Refs. [10,13]. The multilayer system consisted of Ta(1.5 nm)Pd(3 nm)[Co(0.5 nm)Pd(0.7 nm)]$_{40}$Pd(2 nm) layers fixed on the Si_3N_4 membrane. A similar magnetic system was also used in [15]. For pumping and probing the system, linearly polarized x-ray pulses of 778 ± 0.1 eV energy (monochromatized and tuned to the Co L_3-edge absorption resonance) were applied. Their duration was 50 fs FWHM. The sample was covered by a radiation-opaque gold plate with a central hole with a 1.45 μm diameter. X-ray free-electron laser pulses were focused onto the gold plate to a spot size of 10 μm FWHM. However, only a fraction of radiation arrived at the sample, i.e., the fraction passing through the central hole in the plate. We have checked that the average pulse fluence in the aperture (i.e., the fraction of beam energy passing through the aperture, divided by the aperture size) was very similar to the average pulse fluence on the whole sample. The gold plate also had a few small holes outside the sample. The resulting x-ray diffraction patterns were recorded with a CCD detector. From the patterns, the relative diffraction contrast of magnetic speckles was extracted for various values of the x-ray fluence. The result was presented in Fig. 4(b) of Ref. [13]. This quantity reflected the decrease in the magnetic scattering strength with increasing pulse fluence. Our model predictions will be compared to it later.

III. XSPIN MODEL

In order to follow the x-ray-induced magnetization change in irradiated magnetic material the XSPIN (details are given in Appendix A) code was developed [18] as an extension of the hybrid code XTANT [31,32] (see Appendix B). XTANT is an established simulation tool enabling the study of electronic and structural transitions triggered in solids by x rays. The XSPIN code includes all the predominant processes occurring in solids as a result of x-ray irradiation, i.e., inner-shell and conduction band photoabsorption, Auger decay and collisional (impact) ionization, and electron thermalization. In this work, we consider only electronic damage by x rays, assuming that the x-ray pulse fluence was too low to cause any structural damage resulting in atomic displacements. Although the dose absorbed per Co atom needed to melt it thermally seems rather low, $D_{\mathrm{melt}} = 0.54$ eV/atom, this melting criterion is not directly applicable to the femtosecond regime studied, as a much longer time (approximately a few picoseconds) is needed to fully melt Co after the absorption of D_{melt}. Still, this dose gives a rough indication of the value of absorbed energy at which the processes leading to structural changes in Co can start to play a role.

The foundations of the XSPIN code were described in [18]. There are two electronic subsystems—with spin-up and with spin-down electrons—considered in the model. The band structure for both subsystems is obtained from the density of states $D_\sigma(\epsilon)$ calculated with the Vienna Ab initio Simulation Package (VASP) [33–36]. The energy levels in the low-energy-electron fraction (here, containing electrons with energies less than 15 eV above the Fermi level) are determined from the total spin-polarized density of states $D_\sigma(\epsilon)$ calculated for fcc Co (for the experimental bulk value of the lattice constant, $a = 3.545$ Å [37]; see Fig. 1). The energy $E_{i,\sigma}$ of the ith level for spin-σ electrons is then calculated from the equation $i = \int_{-\infty}^{E_{i,\sigma}} d\epsilon D_\sigma(\epsilon)$ [38]. Note that, here, $D_\sigma(\epsilon)$ is the total density of states for the system investigated (i.e., it is not normalized per the number of atoms in the system). It is assumed that all electrons from the low-energy-electron fraction within both the spin-up and spin-down subsystems stay in a common local thermal equilibrium. Therefore, their occupations on individual energy levels follow the Fermi-Dirac distribution, depending on the actual *common* electronic temperature and the *common* chemical potential. By the assumption of the mutual instant thermalization between both electronic subsystems, we implicitly include spin-flip processes in our model.

After an x-ray pulse starts to interact with a solid material, electrons from spin-up and spin-down subsystems are released

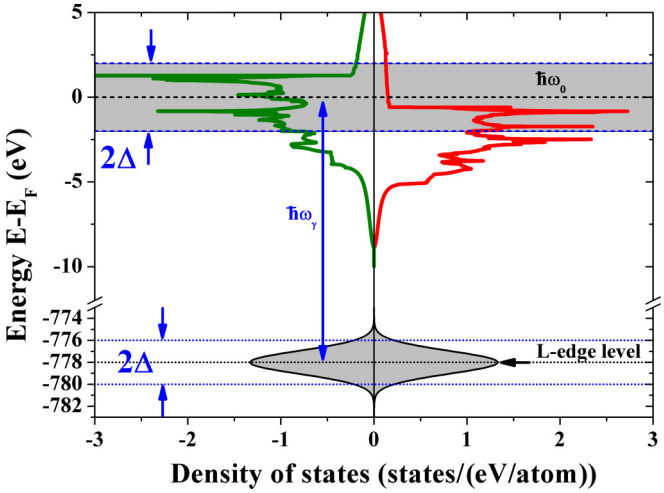

FIG. 1. Calculated density of states (per atom) for equilibrium fcc cobalt, with a schematic indication of the $2p$ band of cobalt and of the probed region in its $3d$ band (the conduction band). The width of the $2p$ band is 2Δ. The density of states is shown for the spin-up domain (red line) and for the spin-down domain (green line).

due to the photoabsorption processes. The excitation probabilities take into account the actual electronic occupations in the respective bands. If the photon energy is sufficiently high to trigger an electronic excitation from a core shell, a spin-up or spin-down electron can be excited from the shell. After the photoabsorption, the energetic photoelectron joins the nonthermalized high-energy-electron fraction (i.e., here, with energies more than 15 eV above the Fermi level). During the sequence of the following impact ionization events, the electron continuously loses energy and, depending on its spin, ultimately joins either the spin-up or spin-down subsystem of the low-energy-electron fraction. The high-energy electrons may collisionally excite secondary electrons with the same or opposite spins. The probability of such an excitation depends on the actual occupation of the spin-up and spin-down electron levels. Core holes relax via Auger decay. A band electron with the same spin fills the hole, while the Auger electron is chosen randomly, according to the actual distribution of spin-up and spin-down electrons. In the code, at each time step an intrinsic averaging over 100 000 different Monte Carlo realizations of electron and hole trajectories is performed in order to calculate the average electronic distribution.

The XSPIN code also provides information on the strength of the resonant magnetic signal, scattered from the x-ray irradiated sample, i.e., the magnetic scattering efficiency $S(F)$. It is equal to the convolution of the incoming beam intensity and the actual magnetization of the sample [16,18,39]:

$$S(F) = \int_{-\infty}^{+\infty} dt\, I(t) M^2(t), \tag{1}$$

where the time-dependent magnetization $M(t)$ reflects the disparity between electronic populations at the resonant states in spin-up and spin-down electronic subsystems:

$$M(t) = \sum_{\hbar\omega_0-\Delta}^{\hbar\omega_0+\Delta} [N_\uparrow^{\text{hole}}(E_{i,\uparrow}) - N_\downarrow^{\text{hole}}(E_{i,\downarrow})], \tag{2}$$

with $N_\sigma^{\text{hole}}(E_{i,\sigma})$ denoting the number of empty states at the $E_{i,\sigma}$ level. The XSPIN code calculates transient changes of $N_\sigma^{\text{hole}}(E_{i,\sigma})$ in response to a specific x-ray pulse for the probed energy levels within the Co $2p$ band, i.e., within the interval $\pm\Delta$ around the probed level $\hbar\omega_0$ (Fig. 1). To explain it in more detail, the incoming x-ray photons of energy $\hbar\omega_\gamma$ excite electrons from the $2p$ levels to the $3d$ band (the conduction band). The region in the $3d$ band to which electrons are excited then extends from $\hbar\omega_0 - \Delta$ to $\hbar\omega_0 + \Delta$, where $\hbar\omega_0$ is the difference between the photon energy and the position of the L edge: $\hbar\omega_0 = \hbar\omega_\gamma - E_{\text{edge}}$, with $E_{\text{edge}} = 778$ eV for the L edge of Co. Here, 2Δ is the $2p$ bandwidth, which determines the number of states probed in the $3d$ band. The number of holes within the probed interval of the conduction band then determines the strength of the recorded magnetic signal. Such a definition is a generalization of the standard definition of magnetization, where, for convenience, we calculate the difference between the unoccupied states (holes), instead of the difference between the occupied states (electrons).

IV. RESULTS

For photon energy tuned slightly above the L edge of Co ($E_\gamma = 778.2$ eV), the attenuation length of x rays is 73.09 nm in Co, 73.40 nm in Pd, and 99.89 nm in Ta [40]. If we compare these numbers with the overall size of the multilayer system used in the experiment [13], we can conclude that the x-ray energy is absorbed, to a large extent, homogeneously in the sample. In addition, energetic electrons emitted as a result of photoabsorption spread out on large distances within the sample (the electron ranges are 7.0 nm for Co and 7.5 nm for Pd). This additionally reinforces the homogeneity of the energy distribution in the sample. Therefore, we can estimate and use the same average effective absorbed dose for each of the Co layers. Assuming the homogeneous distribution of secondary electrons in the whole sample after the electron transport, the effective dose corresponds to the average dose absorbed per Co atom needed to create the estimated average number of electrons in a Co layer. We estimated the linear conversion factor between the effective pulse fluence (incoming on the uppermost Ta layer) and the average dose absorbed by Co atoms (which is an input parameter for XSPIN): 1000 mJ/cm^2 corresponds to approximately 8.11 eV/atom. This finding is in contrast to the XSPIN calculations in [18], where the energy absorption was strongly inhomogeneous in the multilayer system, even after the interlayer electron transport was included.

XSPIN simulations were performed for supercells with periodic boundary conditions consisting of 512 atoms of Co. This number of atoms ensured stability and convergence of the calculations. The atomic positions corresponded to the atomic positions in the equilibrium fcc cobalt. Atoms were kept frozen; that is, no x-ray-induced structural modifications in Co or Pd were taken into account. With the XSPIN predictions obtained for time-dependent magnetization $M(t)$ at various values of the absorbed dose, we calculated the magnetic scattering signal $S(F)$. Figure 2 presents the results for the normalized magnetic scattering signal at $\Delta = 2.0$ eV. This Δ value corresponds to the half of the FWHM of the Co L-edge resonance peak [23,24,41,42]. Like in [18], the

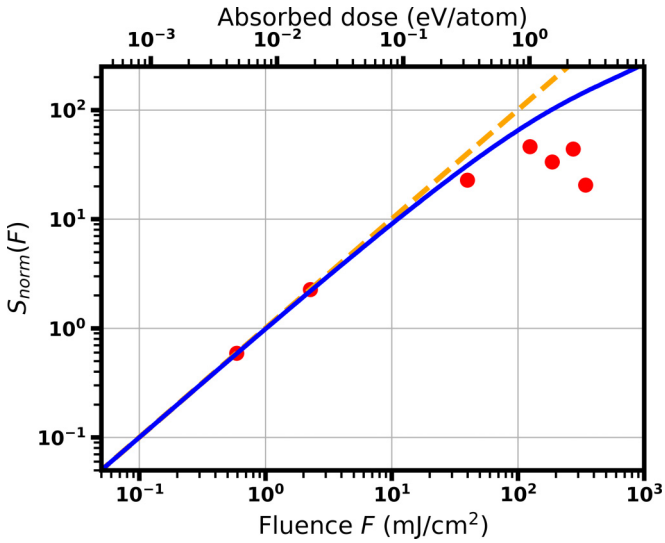

FIG. 2. Normalized magnetic scattering efficiency $S_{\text{norm}}(F)$ as a function of the average absorbed dose, also converted into the effective pulse fluence (incoming on the uppermost Ta layer). Predictions including the demagnetization (blue solid line) and predictions assuming no demagnetization, i.e., $M(t) = M(0)$ (orange dashed line), are shown for comparison. Experimental data (red circles) are taken from Ref. [13]. The value of $\Delta = 2$ eV was used [23,24].

normalized signal is defined as $S_{\text{norm}}(F) = S(F)[F_0/S(F_0)]$, where $F_0 = 0.01$ mJ/cm^2. One can initially see a linear increase of $S_{\text{norm}}(F)$ with the pulse fluence. At doses above 0.24 eV/atom (fluences higher than 30 mJ/cm^2), the curve starts to bend down and becomes nonlinear, similar to what was observed in [18]. The results are compared with the experimental data from [13] after converting the dose into pulse fluence arriving at the Ta upper layer. There is a disagreement between the data and theory predictions at higher fluence values. This is the regime above the structural damage threshold (0.54 eV/atom) where the frozen-atom approximation may be not fully applicable, even at the short timescales considered.

In order to understand the processes behind the change in the magnetic scattering signal observed, we analyzed the simulation results in detail. Figure 3 presents the temporal evolution of the electron temperature, the transient number of excited electrons (with energies above the Fermi level) per atom, and a typical shape of the demagnetization curve $M^2(t)$ obtained for $\Delta = 2.0$ eV and normalized to its initial value. The temporal Gaussian profile of the x-ray pulse with a duration of 50 fs FWHM is also shown. The absorbed dose was, in this case, 0.93 eV/atom. For this dose, one observes a 55% decrease of $M^2(t)$ compared with its initial value at $t = 0$ fs. The decrease in the magnetization is related to the increase in the number of excited electrons [i.e., the electrons with energy above the Fermi level; Fig. 3(b)] and the increase of electronic temperature [Fig. 3(a)]. It is clearly seen [Fig. 3(b)] that more spin-down (minority-spin) electrons are excited than spin-up (majority-spin) electrons. This is due to the "asymmetry" between spin-up and spin-down bands (Fig. 1), i.e., the different density of states for each spin orientation and the different energy level structure in each spin domain. For the spin-down domain, more energy levels are available above the Fermi level, and consequently, more electrons get excited there. We have checked that although the numbers of spin-down and spin-up electrons are different, the energy absorbed in each of the electronic subsystems is comparable, as expected.

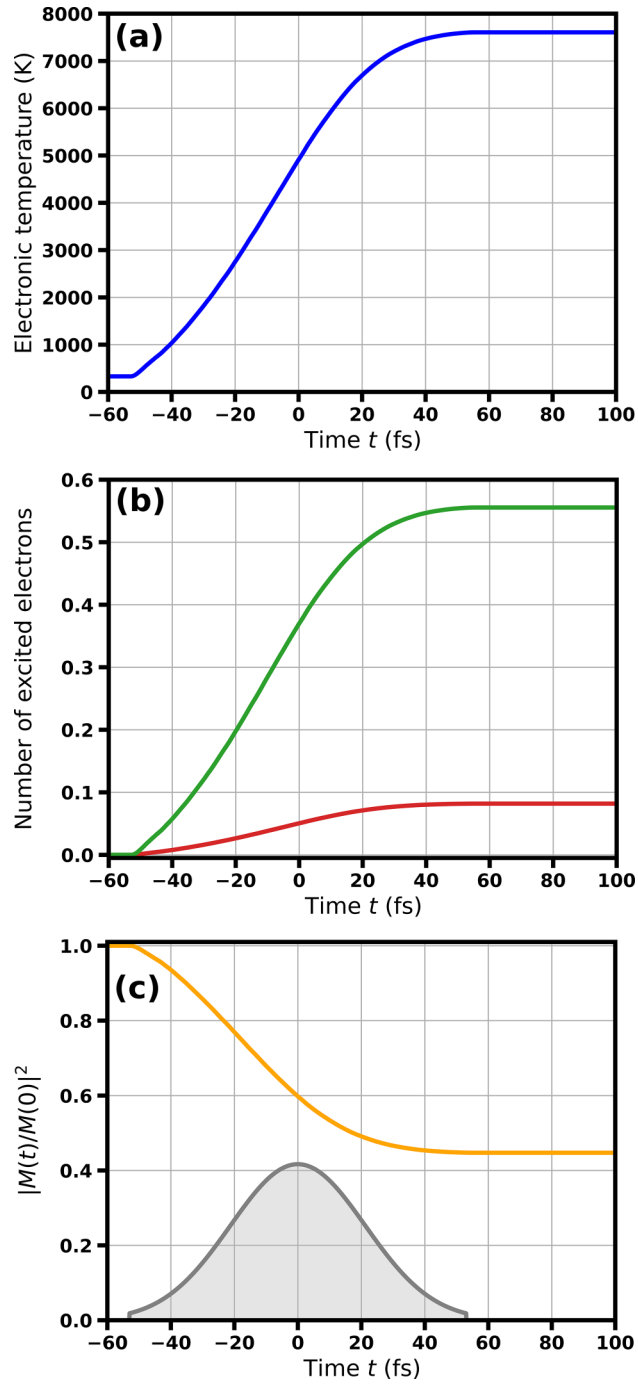

FIG. 3. Temporal evolution of (a) electronic temperature and the (b) number of excited electrons (per atom) in the spin-up and spin-down domains. The red line denotes the spin-up (majority-spin) electron fraction, and the green line denotes the spin-down (minority-spin) electron fraction. (c) Magnetization, with a schematically plotted x-ray pulse shape. The average absorbed dose used for this simulation was 0.93 eV/atom. The value of $\Delta = 2.0$ eV was used for (c) [23,24].

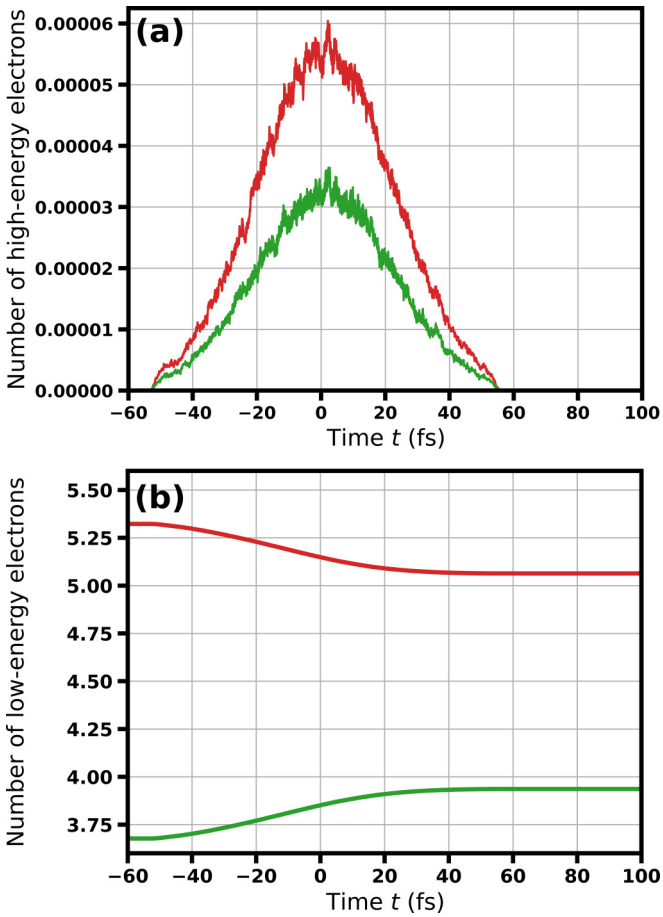

FIG. 4. (a) Number of high-energy electrons and (b) number of low-energy electrons (both per atom) as a function of time. The red line denotes the spin-up (majority-spin) electron fraction, and the green line denotes the spin-down (minority-spin) electron fraction. The results were obtained for the average absorbed dose of 0.93 eV/atom.

In Fig. 4, we present the time evolution of the total number of high-energy electrons (with energies above 15 eV) and low-energy electrons (with energies below 15 eV) normalized per atom. The number of high-energy electrons is relatively small, and its evolution follows the intensity profile of the x-ray pulse. The transient number of high-energy spin-up electrons is larger than the number of high-energy spin-down electrons [Fig. 4(a)]. Still, due to the above-mentioned asymmetry between spin-up and spin-down bands, more electrons get excited to the low-energy spin-down domain during the collisional relaxation of high-energy electrons [Fig. 4(b)]. As a result, the total number of spin-up electrons in the low-energy domain decreases, and the total number of spin-down electrons respectively increases. Ultimately, this drives the change in Co magnetization, as depicted in Fig. 3(c). Note that, when electron cascading saturates, the value of $|M(t)|^2$ stabilizes, here within ∼55 fs after the pulse maximum. As we can see in Fig. 4(a), all high-energy electrons relax by this time into the band, and they just occupy the levels above the Fermi level. Due to ongoing exchange between the electronic system and lattice, the electrons will later lose more energy and finally thermalize with the lattice. However, this will happen on a picosecond timescale, i.e., outside the time window of the experiment and of the current simulation. Therefore, in our model, we do not treat the electron-lattice energy exchange [18].

V. CONCLUSIONS

In summary, we analyzed the role of electronic processes for ultrafast demagnetization in cobalt, triggered by x-ray photons tuned to the *L* edge of Co. The simulations performed with our computational tool XSPIN (which was already successful in describing the magnetization dynamics triggered by photons tuned to the *M* edge of Co [18]), when compared to the *L*-edge data recorded a few years ago at the LCLS facility [13], proved a strong effect of electronic processes also in this case. More experimental data are needed for model validation in the "destructive" fluence regime (i.e., for absorbed doses >0.54 eV/atom). However, it is already clear that the x-ray-driven ultrafast rearrangement of electronic occupations within the magnetically sensitive bands of cobalt strongly impacts its magnetic properties. This observation opens a pathway towards quantitative control and manipulation of x-ray-induced magnetic processes on femto- to picosecond timescales.

ACKNOWLEDGMENTS

B.Z. thanks A. Scherz and S. Parchenko for helpful discussions. K.J.K. thanks the Polish National Agency for Academic Exchange for funding in the frame of the Bekker program (PPN/BEK/2020/1/00184). K.J.K. is also grateful for the funding from the scholarships of the Minister of Science and Higher Education (Poland) for outstanding young scientists (2019 edition, No. 821/STYP/14/2019). V.T. and B.Z. acknowledge the funding received from the Collaboration Grant of the European XFEL and the Institute of Nuclear Physics, Polish Academy of Sciences.

APPENDIX A: SPECIFIC FEATURES OF XSPIN MODEL

XSPIN's hybrid approach enables computationally inexpensive simulations of relatively large supercells (containing up to 1000 atoms). The simulation scheme is based on the code XTANT (for details, see Appendix B). The code treats all predominant electronic and hole core excitation and relaxation processes within an x-ray FEL irradiated sample and follows the sample's nonequilibrium and equilibrium evolution stage. Two electron distributions (with spins up and spins down) are evolved.

The band structure levels in XSPIN are calculated with the VASP (Vienna Ab initio Simulation Package) code for materials in equilibrium [33–36]. VASP is a code which enables high-precision density functional theory calculations for various materials. When applying this equilibrium calculation, we assume that the incoming x-ray pulses are not intense enough to cause any atomic displacements in the magnetic material during the exposure. We also neglect eventual shifts of electronic levels due to high electron temperature. As the nuclei positions are fixed, we can then use the *ab initio* density of states obtained for the material in equilibrium.

A dedicated band structure module calculates the transient electronic occupations of the thermalized electrons. Electron occupation numbers, distributed on the transient energy levels, are assumed to follow the Fermi-Dirac distribution with a transient temperature and chemical potential evolving in time. The electron temperature and electron number change due to the interaction of band electrons with x rays and high-energy electrons. We assume that all band electrons (from both the spin-up and spin-down fractions) undergo instantaneous thermalization at each time step. The intraband collisions, which lead to the electron thermalization, also include spin-flip collisional processes between spin-up and spin-down electrons. In such a way, the spin-flip processes are implicitly included in our model.

The nonequilibrium fraction of high-energy electrons and Auger decays of core holes are treated with a classical event-by-event Monte Carlo simulation. It stochastically models x-ray-induced photoelectron emission from deep shells or from the valence band, the Auger decays, and the scattering of high-energy electrons. In the code, at each time step an intrinsic averaging over 100 000 different Monte Carlo realizations of electron (and core hole) trajectories is performed in order to calculate the average electronic distribution which is then applied at the next time step.

More specific model details are as follows.

(i) In XSPIN, we assume that the x-ray fluences applied do not cause significant structural damage to the material during or shortly after the XUV pulse, i.e., on ∼100 fs timescales. We give the justification below. First, a rigorous definition of the structural damage threshold is difficult at the 100 fs timescale considered. The usual measure for a damage threshold in a metal is the threshold dose for its thermal melting. This dose for cobalt is estimated as 0.54 eV/atom. However, the thermal melting would require picosecond(s) to complete. This time is needed for a transfer of a sufficient amount of energy from the electronic system to the lattice. At the 100 fs timescale, we can use this threshold dose as an indicator only when structural modifications can start to play a role. Second, the usual timescale of atomic displacements during the structural transformation is longer than the femtosecond pulse duration (see, e.g., [43–46]). Both observations guarantee a reasonable modeling accuracy even for doses a few times higher than 0.54 eV/atom on the 100 fs timescales. However, at higher absorbed x-ray doses or when the model is applied at picosecond timescales (e.g., in order to follow the recovery of the magnetization), the possible atomic relocations should be taken into account. Such an extension of XSPIN is possible, but it would require a significant modification of the already complex code, with much effort to be invested. Still, we plan this effort in the future.

(ii) We assume that all band electrons (from both the spin-up and spin-down fractions) undergo instantaneous thermalization at each time step. The intraband collisions, which lead to the electron thermalization, also include spin-flip collisional processes between spin-up and spin-down electrons (cf. [5]). In such a way, the spin-flip processes are implicitly included in our model. Electron-ion coupling is neglected here due to the ultrashort timescales considered. Note that the assumption of instantaneous electron thermalization limits the applicability of XSPIN to model x-ray irradiation with x-ray pulses with a duration longer than the timescale of electronic thermalization. We have performed dedicated simulations with the XCASCADE(3D) code [47] to investigate the timescale of electron cascading process in Co, which is comparable to the timescale of electron thermalization. This indicates that the XSPIN model should not be applied for subfemtosecond x-ray pulses [18].

(iii) For the XSPIN analysis, we used average fluence values estimated by the experiment [13]. They were estimated knowing the beam energy focused on a FWHM focal spot. We assumed that the spatial profile of the x-ray pulse in our simulations was a flat top, with an average fluence. Assuming a homogeneous distribution of secondary electrons in the whole sample after the electron transport, the effective dose corresponds to the average dose absorbed per Co atom needed to create the estimated average number of electrons in a Co layer. Note that attenuation lengths for Ta, Co, and Pd are as follows: $\lambda_{\mathrm{Ta}} = 99.89$ nm, $\lambda_{\mathrm{Co}} = 73.09$ nm, and $\lambda_{\mathrm{Pd}} = 73.40$ nm [40]; that is, they are longer than the multilayer sample thickness (54.50 nm). Therefore, no in-depth volume integration of the signal was performed (compare with [18]).

(iv) XSPIN simulations were performed for the supercell containing 512 Co atoms. As we consider fluences and timescales low enough not to cause atomic relocations, this number of atoms is sufficient to get statistically reliable results. This expectation was confirmed by the preceding convergence tests of our results with respect to the size of the supercell (not shown).

(v) Interactions between magnetic domains in the (X, Y) plane are not included, consistent with the Stoner-Wolfarth model framework of a single magnetic domain [48,49] used here. Results from a simplistic model with periodic domains (not shown) indicate that the details of the domain structure in the (X, Y) plane should not significantly affect our results on 100 fs timescales.

APPENDIX B: MODELING INTERACTIONS OF X RAYS WITH SOLIDS USING XTANT CODE

Modeling radiation damage in nanoscopic samples and solid materials was performed for several years with various simulation techniques (e.g., [31,50–52]). One of the tools is the hybrid code XTANT (X-ray-induced Thermal And Nonthermal Transitions) [31,32,53–55]. Using periodic boundary conditions, XTANT can simulate evolution of x-ray-irradiated bulk materials. The code consists of a few modules dedicated to simulating various processes induced by the incoming x-ray FEL radiation.

(i) The core of the XTANT model is a band structure module (in [31,32,54,55] based on the transferable tight-binding Hamiltonian and in [56] replaced by the DFTB+ code [57]) which calculates the transient electronic band structure of thermalized electrons and the atomic potential energy surface. The latter also evolves in time, depending on the positions of atoms in the simulation box, and is used to calculate the actual forces acting on nuclei.

(ii) After the forces act on atoms, the atoms move. Their actual positions are propagated in time, using a classical molecular dynamics scheme. It solves Newton equations for

the nuclei, with the potential energy surface evaluated from the band structure module.

(iii) Electron occupation numbers, distributed on the transient energy levels, are assumed to follow a Fermi-Dirac distribution with a transient temperature and chemical potential evolving in time. The electron temperature changes due to the interaction of band electrons with x rays and high-energy electrons or due to their nonadiabatic interaction with nuclei (through electron-ion scattering [54]).

(iv) The nonequilibrium fraction of high-energy electrons and Auger decays of core holes are treated with a classical event-by-event Monte Carlo simulation. It stochastically models x-ray-induced photoelectron emission from deep shells or from the valence band, the Auger decays, and the scattering of high-energy electrons. In the code, at each time step an intrinsic averaging over 100 000 different Monte Carlo realizations of electron (and core hole) trajectories is performed in order to calculate the average electronic distribution, which is then applied at the next time step. Ballistic electrons are considered to be high-energy electrons. In the simulated bulk material, they propagate with the restriction of periodic boundaries.

(v) Electron-ion energy exchange can be calculated using a nonadiabatic approach [54]. This energy is transferred to atoms by the respective velocity scaling at each molecular dynamics step.

[1] E. Beaurepaire, J.-C. Merle, A. Daunois, and J.-Y. Bigot, Ultrafast Spin Dynamics in Ferromagnetic Nickel, Phys. Rev. Lett. **76**, 4250 (1996).

[2] B. Koopmans, G. Malinowski, F. D. Longa, D. Steiauf, M. Fahnle, T. Roth, M. Cinchetti, and M. Aeschlimann, Explaining the paradoxical diversity of ultrafast laser-induced demagnetization, Nat. Mater. **9**, 259 (2010).

[3] A. Kirilyuk, A. V. Kimel, and T. Rasing, Ultrafast optical manipulation of magnetic order, Rev. Mod. Phys. **82**, 2731 (2010).

[4] M. Battiato, K. Carva, and P. M. Oppeneer, Superdiffusive Spin Transport as a Mechanism of Ultrafast Demagnetization, Phys. Rev. Lett. **105**, 027203 (2010).

[5] K. Carva, M. Battiato, and P. M. Oppeneer, *Ab Initio* Investigation of the Elliott-Yafet Electron-Phonon Mechanism in Laser-Induced Ultrafast Demagnetization, Phys. Rev. Lett. **107**, 207201 (2011).

[6] M. Battiato, K. Carva, and P. M. Oppeneer, Theory of laser-induced ultrafast superdiffusive spin transport in layered heterostructures, Phys. Rev. B **86**, 024404 (2012).

[7] D. Sander, S. O. Valenzuela, D. Makarov, C. H. Marrows, E. E. Fullerton, P. Fischer, J. McCord, P. Vavassori, S. Mangin, P. Pirro, B. Hillebrands, A. D. Kent, T. Jungwirth, O. Gutfleisch, C. G. Kim, and A. Berger, The 2017 magnetism roadmap, J. Phys. D **50**, 363001 (2017).

[8] C. Gutt, S. Streit-Nierobisch, L.-M. Stadler, B. Pfau, C. M. Günther, R. Könnecke, R. Frömter, A. Kobs, D. Stickler, H. P. Oepen, R. R. Fäustlin, R. Treusch, J. Feldhaus, E. Weckert, I. A. Vartanyants, M. Grunze, A. Rosenhahn, T. Wilhein, S. Eisebitt, and G. Grübel, Single-pulse resonant magnetic scattering using a soft x-ray free-electron laser, Phys. Rev. B **81**, 100401(R) (2010).

[9] B. Pfau *et al.*, Ultrafast optical demagnetization manipulates nanoscale spin structure in domain walls, Nat. Commun. **3**, 1100 (2012).

[10] T. Wang *et al.*, Femtosecond Single-Shot Imaging of Nanoscale Ferromagnetic Order in Co/Pd Multilayers Using Resonant X-Ray Holography, Phys. Rev. Lett. **108**, 267403 (2012).

[11] L. Müller *et al.*, Breakdown of the X-Ray Resonant Magnetic Scattering Signal during Intense Pulses of Extreme Ultraviolet Free-Electron-Laser Radiation, Phys. Rev. Lett. **110**, 234801 (2013).

[12] J. Stöhr and A. Scherz, Creation of X-Ray Transparency of Matter by Stimulated Elastic Forward Scattering, Phys. Rev. Lett. **115**, 107402 (2015).

[13] B. Wu, T. Wang, C. E. Graves, D. Zhu, W. F. Schlotter, J. J. Turner, O. Hellwig, Z. Chen, H. A. Dürr, A. Scherz, and J. Stöhr, Elimination of X-Ray Diffraction through Stimulated X-Ray Transmission, Phys. Rev. Lett. **117**, 027401 (2016).

[14] F. Willems, C. von Korff Schmising, D. Weder, C. M. Günther, M. Schneider, B. Pfau, S. Meise, E. Guehrs, J. Geilhufe, A. E. D. Merhe, E. Jal, B. Vodungbo, J. Lüning, B. Mahieu, F. Capotondi, E. Pedersoli, D. Gauthier, M. Manfredda, and S. Eisebitt, Multi-color imaging of magnetic Co/Pt heterostructures, Struct. Dyn. **4**, 014301 (2017).

[15] Z. Chen, D. J. Higley, M. Beye, M. Hantschmann, V. Mehta, O. Hellwig, A. Mitra, S. Bonetti, M. Bucher, S. Carron, T. Chase, E. Jal, R. Kukreja, T. Liu, A. H. Reid, G. L. Dakovski, A. Föhlisch, W. F. Schlotter, H. A. Dürr, and J. Stöhr, Ultrafast Self-Induced X-Ray Transparency and Loss of Magnetic Diffraction, Phys. Rev. Lett. **121**, 137403 (2018).

[16] M. Schneider, B. Pfau, C. M. Günther, C. von Korff Schmising, D. Weder, J. Geilhufe, J. Perron, F. Capotondi, E. Pedersoli, M. Manfredda, M. Hennecke, B. Vodungbo, J. Lüning, and S. Eisebitt, Ultrafast Demagnetization Dominates Fluence Dependence of Magnetic Scattering at Co *M* Edges, Phys. Rev. Lett. **125**, 127201 (2020).

[17] A. Philippi-Kobs, L. Müller, M. Berntsen, W. Roseker, M. Riepp, K. Bagschik, J. Wagner, R. Frömter, M. Danailov, F. Capotondi, E. Pedersoli, M. Manfredda, M. Kiskinova, M. Stransky, V. Lipp, A. Scherz, B. Ziaja, H. P. Oepen, and G. Grübel, Ultrafast demagnetization excited by extreme ultraviolet light from a free-electron laser, Research Square, preprint rs.3.rs-955056 (2021); https://doi.org/10.21203/rs.3.rs-955056/v1.

[18] K. J. Kapcia, V. Tkachenko, F. Capotondi, A. Lichtenstein, S. Molodtsov, L. Mueller, A. Philippi-Kobs, P. Piekarz, and B. Ziaja, Modeling of ultrafast x-ray induced magnetization dynamics in magnetic multilayer systems, npj Comput. Mater. **8**, 212 (2022).

[19] W. Ackermann *et al.*, Operation of a free-electron laser from the extreme ultraviolet to the water window, Nat. Photonics **1**, 336 (2007).

[20] P. Emma *et al.*, First lasing and operation of an ångstrom-wavelength free-electron laser, Nat. Photonics **4**, 641 (2010).

[21] D. Pile, First light from SACLA, Nat. Photonics **5**, 456 (2011).

[22] E. Allaria *et al.*, Highly coherent and stable pulses from the FERMI seeded free-electron laser in the extreme ultraviolet, Nat. Photonics **6**, 699 (2012).

[23] C. T. Chen, Y. U. Idzerda, H.-J. Lin, N. V. Smith, G. Meigs, E. Chaban, G. H. Ho, E. Pellegrin, and F. Sette, Experimental Confirmation of the X-Ray Magnetic Circular Dichroism Sum Rules for Iron and Cobalt, Phys. Rev. Lett. **75**, 152 (1995).

[24] R. Nakajima, J. Stöhr, and Y. U. Idzerda, Electron-yield saturation effects in *L*-edge x-ray magnetic circular dichroism spectra of Fe, Co, and Ni, Phys. Rev. B **59**, 6421 (1999).

[25] J. P. Hill and D. McMorrow, X-ray resonant exchange scattering: Polarization dependence and correlation functions, Acta Crystallogr., Sect. A **52**, 236 (1996).

[26] J. P. Hannon, G. T. Trammell, M. Blume, and D. Gibbs, X-Ray Resonance Exchange Scattering, Phys. Rev. Lett. **61**, 1245 (1988).

[27] F. Capotondi, E. P. N. M. R. H. Menk, G. Passos, L. Raimondi, C. Svetina, G. Sandrin, M. Zangrando, M. Kiskinova, S. Bajt, M. Barthelmess, H. Fleckenstein, H. N. Chapman, J. Schulz, J. Bach, R. Frömter, S. Schleitzer, L. Müller, C. Gutt, and G. Grübel, Invited Article: Coherent imaging using seeded free-electron laser pulses with variable polarization: First results and research opportunities, Rev. Sci. Instrum. **84**, 051301 (2013).

[28] M. Riepp, K. Bagschik, F. Capotondi, R. Frömter, T. Golz, G. Grübel, M. Kiskinova, L. Müller, D. Naumenko, H. Oepen, E. Pedersoli, A. Philippi-Kobs, W. Roseker, R. Rysov, N. Stojanovic, and M. Walther, Ultrafast magnetisation dynamics at the low-fluence limit supported by external magnetic fields, in *39th Free Electron Laser Conference (FEL'19), Hamburg, Germany, 26-30 August 2019* (JACOW Publishing, Geneva, 2019), pp. 574–577.

[29] C. Stamm, T. Kachel, N. Pontius, R. Mitzner, T. Quast, K. Holldack, S. Khan, C. Lupulescu, E. F. Aziz, M. Wietstruk, H. A. Dürr, and W. Eberhardt, Femtosecond modification of electron localization and transfer of angular momentum in nickel, Nat. Mater. **6**, 740 (2007).

[30] M. Hennes *et al.*, Time-resolved XUV absorption spectroscopy and magnetic circular dichroism at the Ni $M_{2,3}$-edges, Appl. Sci. **11**, 325 (2021).

[31] N. Medvedev, H. O. Jeschke, and B. Ziaja, Nonthermal phase transitions in semiconductors induced by a femtosecond extreme ultraviolet laser pulse, New J. Phys. **15**, 015016 (2013).

[32] N. Medvedev, V. Tkachenko, V. Lipp, Z. Li, and B. Ziaja, Various damage mechanisms in carbon and silicon materials under femtosecond X-ray irradiation, 4open **1**, 3 (2018).

[33] The Vienna Ab initio Simulation Package: Atomic scale materials modelling from first principles, https://www.vasp.at.

[34] G. Kresse and J. Hafner, Ab initio molecular-dynamics simulation of the liquid-metal–amorphous-semiconductor transition in germanium, Phys. Rev. B **49**, 14251 (1994).

[35] G. Kresse and J. Furthmüller, Efficient iterative schemes for *ab initio* total-energy calculations using a plane-wave basis set, Phys. Rev. B **54**, 11169 (1996).

[36] G. Kresse and D. Joubert, From ultrasoft pseudopotentials to the projector augmented-wave method, Phys. Rev. B **59**, 1758 (1999).

[37] W. Wang, Z. Hou, R. Lizárraga, Y. Tian, R. P. Babu, E. Holmström, H. Mao, and H. Larsson, An experimental and theoretical study of duplex fcc+hcp cobalt based entropic alloys, Acta Mater. **176**, 11 (2019).

[38] For example, for a 512-atom supercell, the numbers of levels between the bottom of the calculated (conduction) band and the cutoff energy of 15 eV are 3832 for spin-up electrons and 3792 for spin-down electrons.

[39] J. Stöhr and H. C. Siegmann, *Magnetism: From Fundamentals to Nanoscale Dynamics*, Springer Series in Solid-State Sciences, Vol. 152 (Springer, Berlin, 2006).

[40] B. Henke, E. Gullikson, and J. Davis, X-ray interactions: Photoabsorption, scattering, transmission, and reflection at $E = 50 - 30000$ eV, $Z = 1 - 92$, At. Data Nucl. Data Tables **54**, 181 (1993).

[41] A. M. Hibberd, H. Q. Doan, E. N. Glass, F. M. F. de Groot, C. L. Hill, and T. Cuk, Co polyoxometalates and a Co_3O_4 thin film investigated by L-edge X-ray absorption spectroscopy, J. Phys. Chem. C **119**, 4173 (2015).

[42] M. Guo, X. Liu, and R. He, Restricted active space simulations of the metal L-edge X-ray absorption spectra and resonant inelastic X-ray scattering: Revisiting $[Co^{II/III}(bpy)_3]^{2+/3+}$ complexes, Inorg. Chem. Front. **7**, 1927 (2020).

[43] F. Tavella, H. Höppner, V. Tkachenko, N. Medvedev, F. Capotondi, T. Golz, Y. Kai, M. Manfredda, E. Pedersoli, M. J. Prandolini, N. Stojanovic, T. Tanikawa, U. Teubner, S. Toleikis, and B. Ziaja, Soft x-ray induced femtosecond solid-to-solid phase transition, High Energy Density Phys. **24**, 22 (2017).

[44] I. Inoue, Y. Deguchi, B. Ziaja, T. Osaka, M. M. Abdullah, Z. Jurek, N. Medvedev, V. Tkachenko, Y. Inubushi, H. Kasai, K. Tamasaku, T. Hara, E. Nishibori, and M. Yabashi, Atomic-Scale Visualization of Ultrafast Bond Breaking in X-Ray-Excited Diamond, Phys. Rev. Lett. **126**, 117403 (2021).

[45] V. Tkachenko, M. M. Abdullah, Z. Jurek, N. Medvedev, V. Lipp, M. Makita, and B. Ziaja, Limitations of structural insight into ultrafast melting of solid materials with x-ray diffraction imaging, Appl. Sci. **11**, 5157 (2021).

[46] I. Inoue, V. Tkachenko, K. J. Kapcia, V. Lipp, B. Ziaja, Y. Inubushi, T. Hara, M. Yabashi, and E. Nishibori, Delayed Onset and Directionality of X-Ray-Induced Atomic Displacements Observed on Subatomic Length Scales, Phys. Rev. Lett. **128**, 223203 (2022).

[47] V. Lipp, N. Medvedev, and B. Ziaja, Classical Monte-Carlo simulations of x-ray induced electron cascades in various materials, Proc. SPIE **10236**, 102360H (2017).

[48] E. C. Stoner and E. P. Wohlfarth, A mechanism of magnetic hysteresis in heterogeneous alloys, Philos. Trans. R. Soc. London, Ser. A **240**, 599 (1948).

[49] C. Tannous and J. Gieraltowski, The Stoner-Wohlfarth model of ferromagnetism, Eur. J. Phys. **29**, 475 (2008).

[50] B. F. Murphy *et al.*, Femtosecond x-ray-induced explosion of C_{60} at extreme intensity, Nat. Commun. **5**, 4281 (2014).

[51] P. J. Ho *et al.*, The role of transient resonances for ultra-fast imaging of single sucrose nanoclusters, Nat. Commun. **11**, 167 (2020).

[52] K. R. Beyerlein, H. O. Jönsson, R. Alonso-Mori, A. Aquila, S. Bajt, A. Barty, R. Bean, J. E. Koglin, M. Messerschmidt, D. Ragazzon, D. Sokaras, G. J. Williams, S. Hau-Riege, S. Boutet, H. N. Chapman, N. Tîmneanu, and C. Caleman, Ultrafast non-

thermal heating of water initiated by an x-ray free-electron laser, Proc. Natl. Acad. Sci. U.S.A. **115**, 5652 (2018).

[53] N. Medvedev, H. O. Jeschke, and B. Ziaja, Nonthermal graphitization of diamond induced by a femtosecond x-ray laser pulse, Phys. Rev. B **88**, 224304 (2013).

[54] N. Medvedev, Z. Li, V. Tkachenko, and B. Ziaja, Electron-ion coupling in semiconductors beyond Fermi's golden rule, Phys. Rev. B **95**, 014309 (2017).

[55] N. Medvedev and B. Ziaja, Multistep transition of diamond to warm dense matter state revealed by femtosecond x-ray diffraction, Sci. Rep. **8**, 5284 (2018).

[56] V. Lipp, V. Tkachenko, M. Stransky, B. Aradi, T. Frauenheim, and B. Ziaja, Density functional tight binding approach utilized to study x-ray-induced transitions in solid materials, Sci. Rep. **12**, 1551 (2022).

[57] B. Hourahine *et al.*, DFTB+, a software package for efficient approximate density functional theory based atomistic simulations, J. Chem. Phys. **152**, 124101 (2020).